THE JOURNAL OF PHYSICAL CHEMISTRY B

Article

pubs.acs.org/JPCB

Three Entropic Classes of Side Chain in a Globular Protein

Dennis C. Glass,[†,‡] Marimuthu Krishnan,[§] Jeremy C. Smith,[†,∥] and Jerome Baudry*[,†,∥]

[†]UT/ORNL Center for Molecular Biophysics, Oak Ridge National Laboratory, P.O. Box 2008 Oak Ridge, Tennessee 37831-6309, United States

[‡]The Genome Science & Technology Program, The University of Tennessee, Knoxville, Tennessee 37996, United States

[§]Center for Computational Natural Sciences and Bioinformatics, International Institute of Information Technology, Hyderabad 500 032, India

[∥]Department of Biochemistry and Molecular and Cellular Biology, University of Tennessee, M407 Walters Life Sciences, 1414 Cumberland Avenue, Knoxville, Tennessee, United States

Supporting Information

ABSTRACT: The relationship between the NMR methyl group axial order parameter and the side chain conformational entropy is investigated in inhibitor-bound and apo human HIV protease using molecular dynamics simulation. Three distinct entropic classes of methyl-bearing side chains, determined by the topological distance of the methyl group from the protein backbone (i.e., the number of χ-bonds between the C_α and the carbon of the CH_3 group), are revealed by atomistic trajectory analyses performed in the local frame of reference of individual methyl probes. The results demonstrate that topologically equivalent methyl groups experience similar nonbonded microenvironments regardless of the type of residues to which they are attached. Similarly, methyl groups that belong to the same side chain but that are not topologically equivalent exhibit different thermodynamic and dynamic properties. The two-parameter classification (based upon entropy and methyl axial order parameter) of side chains described here permits improved estimates of the conformational entropies of proteins from NMR motional parameters.

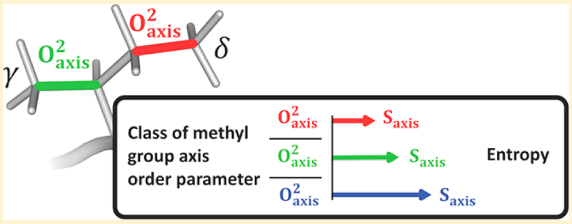

INTRODUCTION

Methyl groups in proteins are markers of the microenvironment and of the thermodynamics of the side chain to which they are attached, and are proxies for global thermodynamic and functional properties of macromolecules.[1−3] Variations in the rotational dynamics of methyl groups arise from microenvironmental effects,[4−6] with relatively large changes in methyl dynamics resulting from small perturbations in the microenvironment.[7−9] For example, ligand binding in calmodulin leads to changes in methyl dynamics that have been used to approximate changes in total protein conformational entropy, which in turn was found to be related to the total binding entropy.[10,11] This has allowed the development of a quantified relationship between methyl group dynamics and protein conformational entropy, resulting in an "entropymeter" probing changes in protein conformational entropy due to high-affinity interactions.[11−13]

NMR spectroscopy is a central experimental approach for the characterization of methyl group dynamics and its response to microenvironmental changes. This characterization is based on a generalized squared order parameter, often labeled S^2 (but termed O^2 here to differentiate it from the entropy "S"), which is a model-free measure of the spatial restriction of the angular motion of an internuclear vector. The value of the order parameter varies from 0 in the case of isotropic motion to 1 when no motion is present.[14,15] Methyl group motion can be decomposed into rotation of the C−H vector around the X_1−C symmetry axis, and reorientational dynamics of the axis itself (Figure 1A).

The order parameter describing the reorientational motion of the X_1−C symmetry axis is labeled O^2_{axis}, and that describing the rotational motion of the C−H vector is labeled O^2_{rot}. Assuming that there is no coupling between the relaxation described by O^2_{rot} and that described by O^2_{axis}, the experimentally determined order parameter O^2 is[14,15]

$$O^2 = O^2_{rot} \cdot O^2_{axis} \quad (1)$$

If the methyl group geometry is assumed to be C_3-symmetric, O^2_{rot} becomes a function of β, the angle between the methyl symmetry axis X_1−C and the C−H bond (Figure 1A). If, furthermore, $\beta = 109.47°$ (ideal tetrahedral geometry of the methyl group), the value of O^2_{rot} is 0.111,[14,15] and in this case the commonly reported order parameter O^2_{axis} is $O^2/0.111$.

Interpreting the NMR-derived O^2_{axis} and its variations in terms of entropy changes involves the selection of a model (e.g., "diffusion in a cone") that is somewhat arbitrary, and a different model may in principle lead to a different estimate of conformational entropy.[16] In addition, information on corre-

Received: January 17, 2013
Revised: February 14, 2013
Published: February 19, 2013

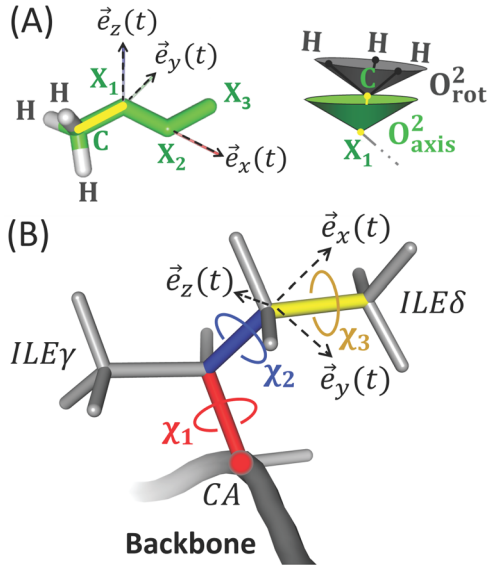

Figure 1. (A) Diagram of a methyl group on a side chain. X_i represents any eligible atom type. A local frame of reference (dashed arrows) is shown spanned by $\vec{e}_x$, $\vec{e}_y$, and $\vec{e}_z$ (see Methods). The origin of the local coordinate system is defined as atom X_1, the local x-axis, $\vec{e}_x$ is aligned with the X_1-X_2 vector, the local $x-y$ plane is spanned by the X_1-X_2 and X_2-X_3 vectors, and the local z-axis is defined by the direction of the cross-product between X_1-X_2 and X_2-X_3 vectors. Part B illustrates the local coordinate system, defined by $\vec{e}_x$, $\vec{e}_y$, and $\vec{e}_z$. Methyl group axis reorientation is illustrated by a green cone, the corresponding order parameter being O^2_{axis}. The methyl group rotational axis is represented by a gray cone. (B) Illustration of an ILE residue. The ILEδ methyl group axis is shown in yellow and the side chain dihedrals χ_1 and χ_2 in red and blue. For ILEδ, a local frame of reference is illustrated, too.

lated motion is not contained in NMR-derived O^2_{axis}, so that the summation over the entropy estimates based on all individual methyl group order parameters may yield only an upper limit to the overall methyl group entropy.[17−19] The choice of a motional model can be avoided by using molecular dynamics (MD) simulations to calculate directly the methyl group entropy and O^2_{axis}.[17]

The contribution of the side chain's internal dynamics to methyl group order parameters has been previously described and the precession of the methyl group's terminal axis, described by O^2_{axis}, found to be correlated with dihedral transitions in the side chain.[20−22] For example, the distribution of O^2_{axis} values for the ILE$_\delta$ methyl group, which is influenced by χ_1 and χ_2 dihedral angle rotameric transitions (Figure 1B), splits into four "classes" depending on whether (i) both the χ_1 and χ_2 dihedral or (ii) only χ_1, or (iii) only χ_2, or (iv) neither χ_1 nor χ_2, undergo rotameric transitions. This is in contrast to the distribution of O^2_{axis} values for the ILEγ methyl group that splits in two "classes" depending on whether or not χ_1 undergoes rotameric transitions (Figure 1B).[21]

In addition to these dihedral fluctuations, the dynamics of a methyl group is to a large extent controlled by its nonbonded microenvironment.[7−9] A detailed understanding of the role of the nonbonded microenvironment in controlling the side chain dynamics is of considerable interest. The present work investigates the contributions of the nonbonded microenvironment of a methyl group to its axis order parameter and associated entropy. For this purpose, the motion of methyl groups is considered in the local frame of reference (see Figure 1B and Methods), thereby eliminating the contributions of other dihedral degrees of freedom to side chain dynamics that would otherwise superpose with those of the nonbonded interactions.

METHODS

Molecular Dynamics Simulations of HIV Protease. Human immunodeficiency virus type 1 protease (HIV PR) is a methyl-rich (44% methyl bearing residues, 75 methyl groups per 99 residue monomer), well-studied system with experimental order parameters available.[23−26] Molecular dynamics simulations of HIV PR were carried out using NAMD 2.6,[27] the CHARMM 27 all-atom force field,[28] and the TIP3P water model.[29] Force field parametrization of the ligand is described below. Molecular dynamics simulations were performed on three different HIV PR systems: (i) wild-type (WT) apo-HIV PR (PDB ID: 2PC0[30]), (ii) wild-type HIV PR with the inhibitor DMP323 bound, a C_2-symmetric cyclic urea,[31] and (iii) mutant (MUT) HIV PR with the cyclic urea inhibitor DMP323 bound (PDB ID: 1QBS[32]). The ligand-bound wild-type starting structure was obtained by mutating the 1QBS sequence back to the 2PC0 wild-type sequence using the program MOE (Chemical Computing Group).[33] The *S*-hydroxy-cysteine in 1QBS was treated as a regular cysteine. Differences in primary sequence between 2PC0 and 1QBS are given in Table S1 (Supporting Information). Both aspartates in the catalytic dyad were modeled as protonated.[34] Other hydrogen atoms were added using the HBUILD facility in CHARMM.

The structures are solvated in a cubic box of TIP3P water ($76 \times 76 \times 76$ Å^3), and neutralized by adding 6 Cl^- ions to systems i and ii and 8 Cl^- ions to system iii. Molecular dynamics simulations were performed in the NPT statistical ensemble at 310 K and 1 atm using a Langevin thermostat with a damping coefficient of 5 ps^{-1}. A switching function was used to smooth nonbonded interactions between 10 and 12 Å. A pairlist distance of 14 Å was used. The particle mesh Ewald method was used for electrostatics with a real space cutoff of 12 Å. Water bond lengths and angles were constrained to their parameter values as defined in the TIP3P model. Protein hydrogen atoms were not constrained. A time-step of 1 fs was used.

Five replicas of each of the three simulation systems were equilibrated for 1 ns at 310 K with different initial velocity assignments. Each replica was simulated for 21 ns, yielding a total of 315 ns production dynamics ($3 \times 5 \times 21$ ns). Coordinates were saved every 100 fs. Error estimates throughout the present paper were made from differences between the replicas for each simulation set.

Ligand Parametrization. Parameters for DMP323 (Figure S4, Supporting Information) not already present in the CHARMM force field were developed following the CHARMM parametrization protocol.[28,35] Energy-minimized geometries were obtained at the B3LYP/6-31G* level of theory using Gaussian 03[36] for DMP323 alone or in complex with various numbers of water molecules in hydrogen-bonding positions (Figure S5, Supporting Information). Gas-phase interaction energies for the corresponding geometries were calculated at the HF/6-31G* level of theory and scaled by 1.16.[28] Missing DMP323 empirical force field parameters and partial charges were iteratively changed to simultaneously reproduce interaction energies (within k_BT) and geometries (within 0.4 Å heavy-atom root-mean-square deviation between QM and MM structures) of the ligand−water complexes. The

dx.doi.org/10.1021/jp400564q | J. Phys. Chem. B 2013, 117, 3127−3134

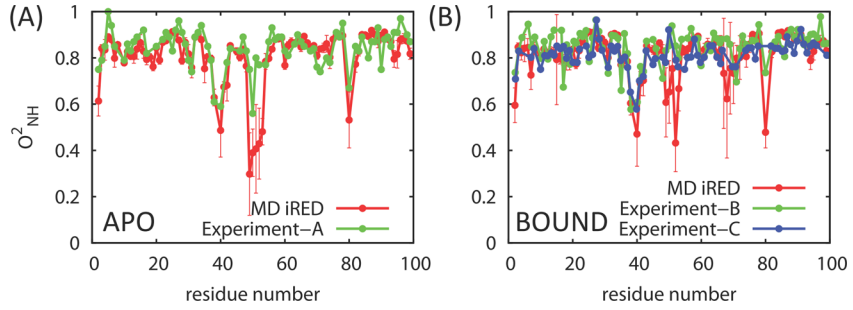

Figure 2. Average backbone amide order parameters O^2_{NH} from MD simulation using the iRED method[37,38] and from experiment. Experimental data A, B, and C from refs 39, 40, and 41, respectively. Error bars correspond to standard deviation around the mean. Apo and bound data from simulations of PDB ID 2PC0 (A) and 1QBS (B), respectively.

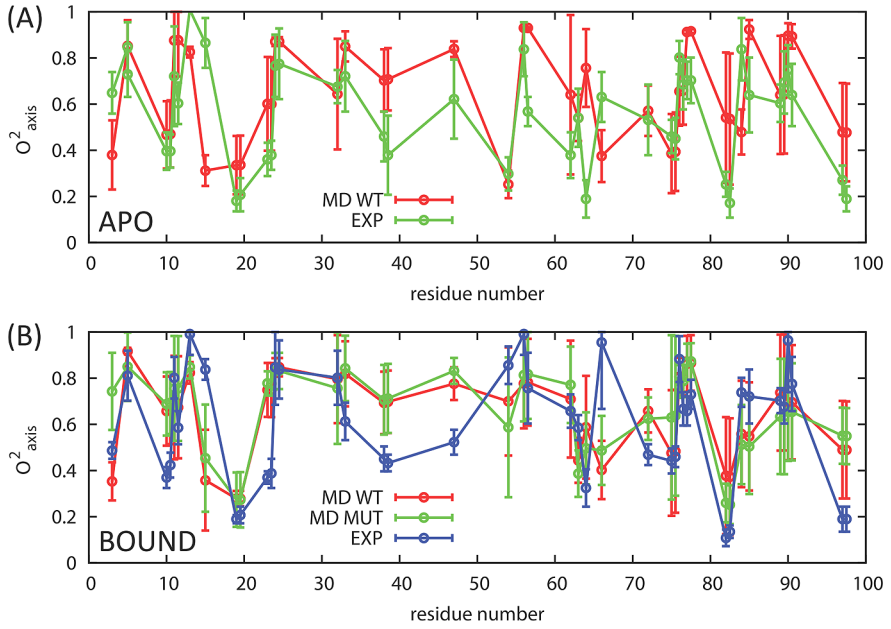

Figure 3. Average side chain order parameters O^2_{axis} from MD simulation and experiment[42] for apo- (A) and ligand-bound (B) systems. Experimental data obtained from a mutant HIV protease.[42] Only residues for which experimental data is available are shown. For residues with two methyl groups, the second order parameter is shown offset by 0.5 in residue number for clarity of presentation.

parameters obtained are listed in Tables S3–S6 (Supporting Information).

Local Methyl Group Frame of Reference. To remove the direct effect of the rotators' internal dynamics on methyl group axis order parameters and entropies, a local frame of reference was used for each methyl group. The coordinates of side chain atoms immediately preceding the methyl group were superimposed for every snapshot of the simulation as in Figure 1. Methyl group motion in this local frame of reference consists only of methyl group axis reorientation (e.g., reorientation of the yellow bond in Figure 1B) and methyl group rotation (e.g., rotation about the χ_3 dihedral in Figure 1B).

Order Parameters from Molecular Dynamics Trajectories. Methyl group axis order parameters, $O^2_{axis,local}$, were calculated as

$$O^2_{axis,local} = \frac{3}{2}(\langle x^2\rangle^2 + \langle y^2\rangle^2 + \langle z^2\rangle^2 + 2\langle xy\rangle^2 + 2\langle xz\rangle^2 + 2\langle yz\rangle^2) - \frac{1}{2} \quad (2)$$

where x, y, and z are the coordinates of the methyl group axis in the local frame of reference described above.

Order parameters were also calculated in a global Cartesian protein frame of reference using the isotropic reorientational eigenmode dynamics (iRED) method.[37,38] The iRED method includes all motion contributing to the experimental order parameter, including side chain dihedrals antecedent to the vector C–X_1 (Figure 1), and backbone motion. The isotropically averaged covariance matrix M was calculated as

$$M_{ij} = \frac{1}{2}\langle 3(\vec{\mu}_i\vec{\mu}_j) - 1\rangle \quad (3)$$

where $\vec{\mu}_i$ (i = 1, ..., N, N is the number of bond vectors) is a normalized bond vector from one MD configuration (e.g., corresponding to a backbone amide or methyl group axis) and $\langle\cdot\rangle$ denotes an ensemble average approximated by an MD time average. Solving the eigenvalue problem

$$M_{ij}|m\rangle = \lambda|m\rangle \quad (4)$$

yields eigenvalues λ_m and eigenvectors $|m\rangle$. The order parameters were calculated over all m' modes corresponding to internal motion as

dx.doi.org/10.1021/jp400564q | J. Phys. Chem. B 2013, 117, 3127–3134

$$O^2_{\text{axis}} = 1 - \sum_{m'} \lambda_{m'} |\|m'\rangle|^2 \quad (5)$$

RESULTS AND DISCUSSION

Validation of the Molecular Dynamics Simulations. Order parameters were calculated from five replicas of every system (WT-apo, WT-bound, MUT-bound) using the iRED method (eq 5). Figure 2 compares the calculated average backbone amide order parameters, O^2_{NH}, with experimental values.[39−41] The apo simulation and experimental results are in agreement, with only the flexibility of the protein flaps (residues 49−54) being higher in the simulation than in the experiment (Figure 2A). Upon ligand binding, order parameters in the flap region increase, indicating flap closure and reduced backbone dynamics (Figure 2B) in agreement with site-specific NMR relaxation experiments.[24,25]

The effect of methyl rotation and geometry on O^2_{axis} was examined and indicates that the relaxation described by O^2_{axis} and that described by O^2_{rot} are decoupled and independent (eq 1), as shown in Figure S1 (Supporting Information). Figure 3 compares the iRED calculated side chain order parameters, O^2_{axis}, with experiment[42] for the apo- (Figure 3A) and ligand-bound (Figure 3B) protein. Near-quantitative agreement between simulation and experiment is found within the error margins with some exceptions. Differences between the experimental and simulated O^2_{axis} have been attributed partly to inadequate sampling of the conformational space of side chains and partly to the fact that current force field parameters are not accurate enough to fully capture the realistic dynamics of protein side chains.[21,43]

The methyl group order parameter O^2_{axis} includes, in principle, effects from all protein internal motion. Unlike O^2_{axis}, the quantity $O^2_{\text{axis,local}}$, calculated in the local frame of reference (eq 2), reports exclusively on local methyl group motion. Figure 4 shows that $O^2_{\text{axis,local}}$ strongly correlates with

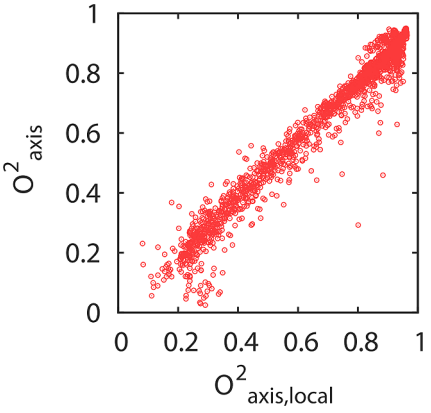

Figure 4. Comparison of methyl group axis order parameters O^2_{axis} and $O^2_{\text{axis,local}}$ calculated in a global and local frame of reference, respectively.

O^2_{axis}, which indicates that order parameters calculated in the local framework indeed represent well the experimentally derived order parameters, O^2_{axis}. Figure 4 also suggests that the motion of the methyl group's symmetry axis in the local methyl frame of reference contributes significantly to the order parameter while other degrees of freedom contribute negligibly.

Entropic Classification of Side Chains. Methyl group axis conformational entropies were calculated in the local frame of reference described above using

$$S_x = -k_B T \int \rho(\vec{\mu}) \ln(\rho(\vec{\mu}))\, d\vec{\mu} \quad (6)$$

where k_B is Boltzmann's constant, T is the temperature (310 K), and $\rho(\vec{\mu})$ is the probability density of the methyl group axis vector $\vec{\mu}$ (=x, y, z). Figure 5A shows S_x plotted against the order

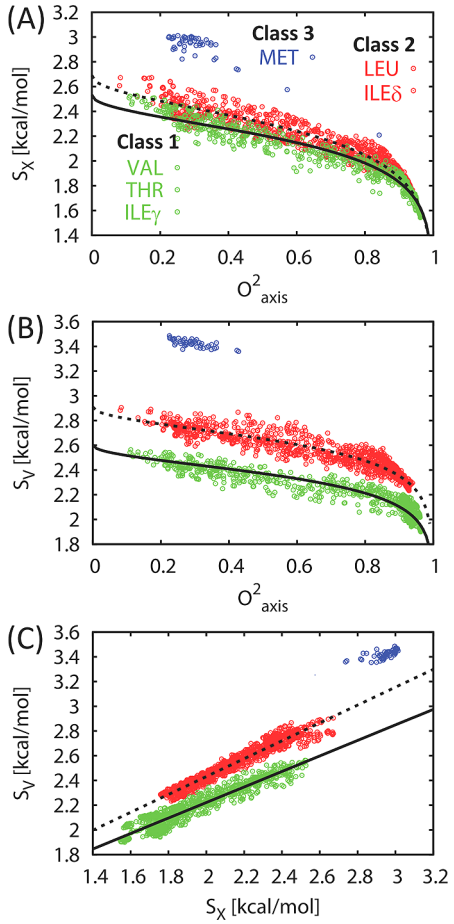

Figure 5. (A) Conformational entropy S_x versus order parameter O^2_{axis}. The probability density, ρ, was obtained by binning the conformations sampled in the MD simulations using a bin size of 0.1 Å. The resulting integrated distribution was normalized to 1 to yield a probability. Bond lengths were considered constant in analogy with NMR order parameter analysis.[14,44] (B) Entropy S_v versus O^2_{axis}. S_v has been calculated with the probability density $\rho(\vec{\mu}_v)$ obtained using a bin width of 1 Å/ps. (C) Conformational entropy S_x versus entropy S_v. One point corresponds to one methyl group. Color distinguishes classes of methyl group. Equation 7 is fitted to the data in panels A and B (full lines). Entropies S_x and S_v were calculated in the local Cartesian methyl group coordinate system.

parameter $O^2_{\text{axis,local}}$ for the methyl group symmetry axis reorientation (X_1−C in Figure 1A). As expected, an inverse relationship between $O^2_{\text{axis,local}}$ and S_x is apparent, i.e., lower methyl group axis fluctuation corresponds to smaller S_x values.

The behavior of the methyl groups can be grouped in three classes. The entropies for ILEγ, THRγ, and VAL$\gamma_{1,2}$ ("class 1") are overall slightly lower than those of ILEδ and LEU$\delta_{1,2}$ ("class 2"), which in turn are lower than those of METε ("class 3"), in agreement with the average free energy barrier to methyl group motion decreasing from classes 1 to 2 to 3.[43] The large values calculated for class 3 (MET) originate from the CHARMM27 dihedral force field parameters as discussed below. Overall, the

dx.doi.org/10.1021/jp400564q | J. Phys. Chem. B 2013, 117, 3127−3134

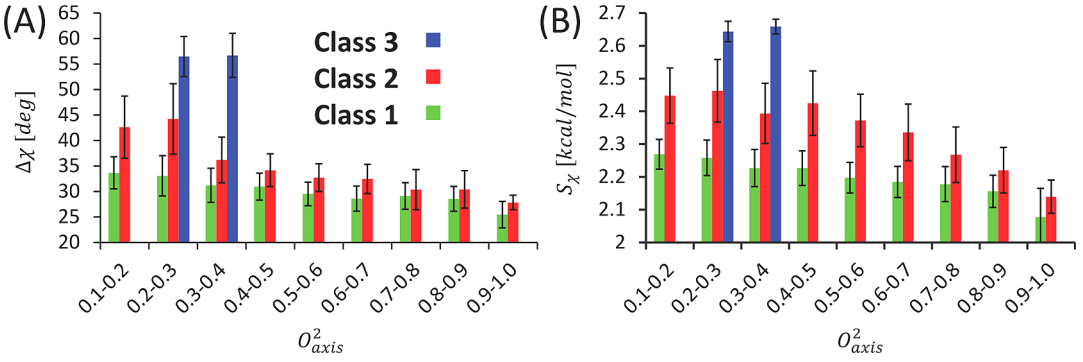

Figure 6. (A) Average width $\Delta\chi$ and (B) Shannon entropy $S\chi$ as a function of order parameter for methyl groups in classes 1−3. Averages taken within ranges of the order parameter as labeled. Error bars represent standard deviation from the mean. The widths of the PMF are calculated as $\Delta\chi = \chi^+ - \chi^-$, where χ^+ and χ^- are the angles at which the PMF is $k_BT \sim 0.6$ kcal/mol (at $T = 310$ K) larger than at its minimum.

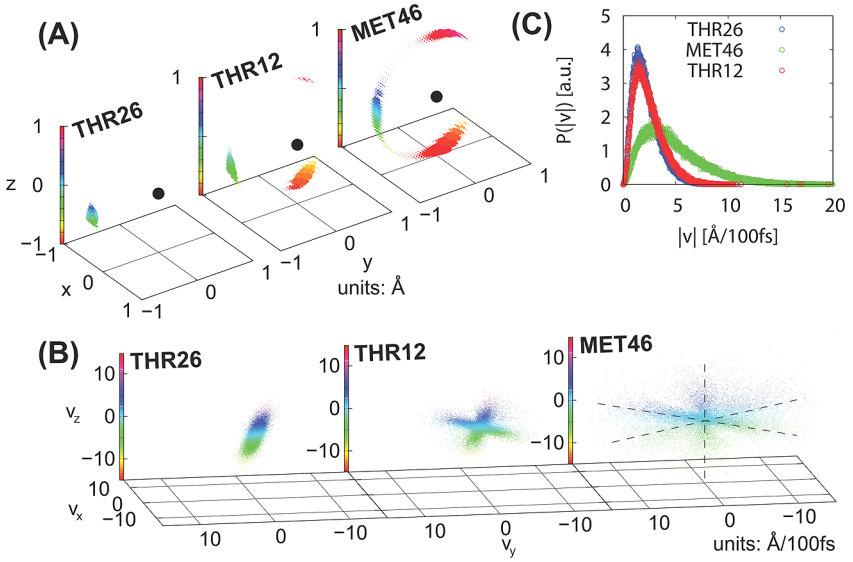

Figure 7. (A) Three-dimensional conformational probability distribution functions $\rho(\vec{x})$ for selected methyl groups. The black point is at the coordinate origin (0,0,0). Points are colored according to their z-coordinate. (B) Three-dimensional velocity probability distribution $\rho(\vec{v})$ for the same three methyl groups as in panel A. Points are colored according to their z-coordinate. Dashed lines illustrate the principal axes of ellipsoids. (C) One-dimensional probability distributions $P(v)$ of the absolute value of the velocity $v = |\vec{v}| = (v_x^2 + v_y^2 + v_z^2)^{1/2}$ using a bin width of 0.01 Å/ps. All distributions were obtained in the local Cartesian methyl group coordinate system.

results indicate that a given value of $O^2_{\text{axis,local}}$ corresponds not to a single entropy value but to a range of entropies and equivalently to a range of disorder of methyl group orientations. The data for classes 1 and 2 were fitted by eq 7:[16]

$$S_x^{\text{fit}} = M \ln(A(3 - \sqrt{1 + 8\sqrt{O_{\text{axis}}{}^2}})) \quad (7)$$

The slope of eq 7 fitted to class 2 is ∼16% larger than when fitted to class 1 (fitting parameters in Table S2, Supporting Information), indicating that types of methyl group (i.e., ILEγ vs ILEδ) need to be distinguished from each other to deduce changes of entropy from changes in order parameter. These findings qualitatively hold also true for order parameters calculated using iRED, i.e., when the influence of all protein internal dynamics is included in the calculation of the order parameters (Figure S2, Supporting Information).

The probability distribution, $\rho(\chi)$, and the corresponding potential of mean force (PMF), $f(\chi) = -k_BT\ln(\rho(\chi))$, around the well-sampled dihedral energy minima are calculated for the three classes of methyl groups. Figure S3 (Supporting Information) shows an example of the thus obtained $\rho(\chi)$ and $f(\chi)$. Figure 6A shows the average width $\Delta\chi$ of the PMF for different ranges of order parameter. For all ranges of order parameter, the value of $\Delta\chi$ increases with topological distance, i.e., the number of χ-bonds between the C_α and the carbon of the CH_3 group. Furthermore, the spread of the probability distribution that determines the PMF can be represented using a Shannon entropy $S_\chi = k_BT\int\rho(\chi)\ln[\rho(\chi)]\,d\chi$. As in the case of $\Delta\chi$, the values of $S\chi$ increase with topological distance (Figure 6B). This suggests that the average shape of the PMF for rotation about the χ dihedrals is sensitive to the methyl group's topological distance from the backbone.

Motional differences between classes of methyl group are also apparent in the distribution of average velocities $\vec{\mu}_v = (v_x, v_y, v_z)$ between two consecutive frames (dt = 100 fs). The extent of this distribution can also be quantified in terms of a Shannon entropy, S_v, calculated using eq 6 and the probability density $\rho(\vec{\mu}_v)$. Figure 5B shows the entropy thus obtained, S_v plotted against $O^2_{\text{axis,local}}$. The data again forms clusters, but these are even more clearly separated than in Figure 5A: VAL$\gamma_{1,2}$, ILEγ, and THRγ ("class 1") exhibit, for a given value of $O^2_{\text{axis,local}}$, smaller S_v values than ILEδ and LEU$\delta_{1,2}$ ("class 2"),

dx.doi.org/10.1021/jp400564q | J. Phys. Chem. B 2013, 117, 3127−3134

which in turn exhibit smaller S_v values than METε ("class 3"), again suggesting distinct classes of methyl group dynamics. Figure 5C shows S_v against S_x. The same classes appear as in the previous panels, suggesting that the methyl group entropies S_v and S_x are correlated in the local frame of reference used here.

Selected probability distribution functions $\rho(x)$ for the axis of the methyl groups (X_1−C in Figure 1) for THR26, MET46, and THR12 are shown in Figure 7. These residues were selected as they exhibit the smallest, largest, and an intermediate conformational entropy, respectively, of the methyl groups in the protein. THR26 exhibits a single cluster of probability density, indicating that the methyl group remains in one conformation during the simulation. THR12 exhibits two main clusters of approximately similar intensity and a third cluster of significantly lesser intensity, indicating that THR12's methyl group mostly explores two conformations. The distribution function for MET46 exhibits three clusters of significant probability and also possesses a relatively large probability density in regions between the clusters, indicating that the MET46 methyl group explores three conformations with frequent transitions between them.

Figure 7B shows the average velocity vector $\vec{\mu}_v = (v_x, v_y, v_z)$ between pairs of consecutive MD snapshots (dt = 100 fs) in the local methyl group frame of reference for the same methyl groups as in Figure 7A. Whereas for THR26 the points are distributed within a single ellipsoid, corresponding to the single conformation explored (Figure 7A), for THR12 the points are distributed over two ellipsoids and for MET46 three, with data points being more spread out than for the THR methyl groups. Figure 7C shows the corresponding probability distributions, $P(v)$, of the absolute value of $\vec{\mu}_v$. The probability distribution $P(v)$ for MET46 is broader than those for the THR methyl groups. Since the probability distributions of the absolute value of $\vec{\mu}_v$ for the two THR methyl groups are largely superimposable, entropies calculated from them would be similar. However, entropies calculated from the three-dimensional probability distributions $\rho^{\mathrm{THR12}}(\vec{\mu}_v)$ and $\rho^{\mathrm{THR26}}(\vec{\mu}_v)$ are in fact different (2.5 and 1.9 kcal/mol, respectively, at 310 K), since $\rho^{\mathrm{THR12}}(\vec{\mu}_v)$ is more spread out in three dimensions than $\rho^{\mathrm{THR26}}(\vec{\mu}_v)$. This suggests a qualitative origin of the relation between S_x and S_v (Figure 5C)—exploring different conformations in coordinate space also increases the distribution of average velocities $\vec{\mu}_v$ between pairs of consecutive MD snapshots (dt = 100 fs) and therefore S_x and S_v increase in a correlated way.

CONCLUSIONS

This work examines methyl group axis order parameters and entropies calculated from molecular dynamics simulation of apo- and bound HIV protease species, removing the contributions of backbone and internal side chain dynamics to the methyl group order parameters. Three classes of methyl group dynamics are identified, with entropies S_x and S_v increasing from class 1 (ILEγ, THRγ, and VAL$\gamma_{1,2}$) to class 2 (ILEδ, LEU$\delta_{1,2}$) to class 3 (METε) in a way that also correlates with side chain length, i.e., the "topological distance" from the backbone (Figure 5A). The present classification differs from the "classes" investigated in refs 21 and 45, which are based on differences in the values of the methyl group O^2_{axis} and arise from the dynamics of the entire side chain. In contrast, the present work classifies methyl groups based on the relation between the order parameters and the corresponding entropy, so that methyl groups that exhibit similar O^2_{axis} can still participate in different classes (Figure 5A). Interestingly, although the contribution of dihedral fluctuations (χ_1 and χ_2) to the internal side chain dynamics has been removed from the methyl group motion, a classification sensitive to the topological position, or distance from the backbone, is still found.

The differences between the classes of methyl group found here do not arise only from the CHARMM27 dihedral force field parameters. The χ_1 dihedral for ILEγ, THRγ, and VALγ1,2 (class 1) and the χ_2 dihedral for ILEδ and LEUδ1,2 (class 2) have the same force constant for the dihedral term, with a barrier of 3.6 kcal/mol, while METε methyl groups have a smaller dihedral term of 1.86 kcal/mol that causes a more smeared-out Boltzmann probability distribution resulting in the relatively large entropy for MET in Figure 5. Despite identical force field parameters for χ_1 and χ_2 dihedrals (Figure 1B), the width of the potentials of mean force for rotation about the χ_1 (for γ methyl groups) and χ_2 (for δ methyl groups) dihedrals differ between the classes 1 and 2 defined in Figure 5A, respectively. Since the order parameter and corresponding entropy of the methyl groups are calculated here in their local frame of reference, where all motions other than that of the methyl group axis have been removed, the differences observed between class 1 and class 2 methyl groups originate from their nonbonded environment. This suggests that not all methyl groups on a given side chain (e.g., ILEγ and ILEδ) behave equally.

However, methyl groups do exhibit similar properties if they share the same topological distance from the backbone. This suggests that the variation of entropy obtained from a variation of the order parameter of a methyl group at one topological position (e.g., ILEγ) will not necessarily be the same as that obtained from a methyl group at a different topological position (e.g., ILEδ) and that methyl groups at different topological positions may respond differently to, e.g., ligand binding. In the present simulations, for example, the difference in conformational entropy between the apo and bound species calculated for the ILEδ and ILEγ methyl groups is 0.05 and 0.11 kcal/mol/methyl (at 310 K), respectively, considering only the ILE residues located in the protein flaps (residue numbers 47, 50, and 54) as only those showed significant changes in conformational entropy upon ligand binding.

ASSOCIATED CONTENT

Supporting Information

Detailed information on the simulation and ligand parametrization protocol together with CHARMM force field parameters for the ligand. This material is available free of charge via the Internet at http://pubs.acs.org.

AUTHOR INFORMATION

Corresponding Author

*E-mail: jbaudry@utk.edu. Phone: (865) 576 0930.

Notes

The authors declare no competing financial interest.

ACKNOWLEDGMENTS

D.C.G. is supported in part by the Graduate School of Genome Science and Technology at the University of Tennessee, Knoxville. J.B. acknowledges a start-up grant from the University of Tennessee, Knoxville. J.C.S. acknowledges

support from the National Science Foundation. M.K. acknowledges support from the Department of Science and Technology (DST), New Delhi.

REFERENCES

(1) Krishnan, M.; Smith, J. C. Response of Small-Scale, Methyl Rotors to Protein-Ligand Association: A Simulation Analysis of Calmodulin-Peptide Binding. *J. Am. Chem. Soc.* **2009**, *131*, 10083−10091.
(2) Lee, A. L.; Kinnear, S. A.; Wand, A. J. Redistribution and Loss of Side Chain Entropy upon Formation of a Calmodulin-Peptide Complex. *Nat. Struct. Biol.* **2000**, *7*, 72−77.
(3) Hajduk, P. J.; Augeri, D. J.; Mack, J.; Mendoza, R.; Yang, J.; Betz, S. F.; Fesik, S. W. NMR-Based Screening of Proteins Containing 13C-Labeled Methyl Groups. *J. Am. Chem. Soc.* **2000**, *122*, 7898−7904.
(4) Hayward, R. L.; Middendorf, H. D.; Wanderlingh, U.; Smith, J. C. Dynamics of Crystalline Acetanilide: Analysis Using Neutron Scattering and Computer Simulation. *J. Chem. Phys.* **1995**, *102*, 5525−5541.
(5) Alvarez, F.; Alegría, A.; Colmenero, J.; Nicholson, T. M.; Davies, G. R. Origin of the Distribution of Potential Barriers for Methyl Group Dynamics in Glassy Polymers: A Molecular Dynamics Simulation in Polyisoprene. *Macromolecules* **2000**, *33*, 8077−8084.
(6) Nair, S.; Dimeo, R. M.; Neumann, D. A.; Horsewill, A. J.; Tsapatsis, M. Methyl Rotational Tunneling Dynamics of P-Xylene Confined in a Crystalline Zeolite Host. *J. Chem. Phys.* **2004**, *121*, 4810.
(7) Baudry, J. Van der Waals Interactions and Decrease of the Rotational Barrier of Methyl-Sized Rotators: A Theoretical Study. *J. Am. Chem. Soc.* **2006**, *128*, 11088−11093.
(8) Baudry, J.; Smith, J. C. Can Proteins and Crystals Self-Catalyze Methyl Rotations? *J. Phys. Chem. B* **2005**, *109*, 20572−20578.
(9) Hembree, W. I.; Baudry, J. Y. Three-Dimensional Mapping of Micro-Environmental Control of Methyl Rotational Barriers. *J. Phys. Chem. B* **2011**, *115*, 8575−8580.
(10) Frederick, K. K.; Marlow, M. S.; Valentine, K. G.; Wand, A. J. Conformational Entropy in Molecular Recognition by Proteins. *Nature* **2007**, *448*, 325−3.
(11) Marlow, M. S.; Dogan, J.; Frederick, K. K.; Valentine, K. G.; Wand, A. J. The Role of Conformational Entropy in Molecular Recognition by Calmodulin. *Nat. Chem. Biol.* **2010**, *6*, 352−358.
(12) Schwalbe, H.; Rinnenthal, J. Thermodynamics: The World is Flat. *Nat. Chem. Biol.* **2010**, *6*, 312−313.
(13) Moorman, V. R.; Valentine, K. G.; Wand, A. J. The Dynamical Response of Hen Egg White Lysozyme to the Binding of a Carbohydrate Ligand. *Protein Sci.* **2012**, *21*, 1066−1073.
(14) Lipari, G.; Szabo, A. Model-Free Approach to the Interpretation of Nuclear Magnetic Resonance Relaxation in Macromolecules. 1. Theory and Range of Validity. *J. Am. Chem. Soc.* **1982**, *104*, 4546−4559.
(15) Lipari, G.; Szabo, A. Model-Free Approach to the Interpretation of Nuclear Magnetic Resonance Relaxation in Macromolecules. 2. Analysis of Experimental Results. *J. Am. Chem. Soc.* **1982**, *104*, 4559−4570.
(16) Yang, D. W.; Kay, L. E. Contributions to Conformational Entropy Arising from Bond Vector Fluctuations Measured from NMR-Derived Order Parameters: Application to Protein Folding. *J. Mol. Biol.* **1996**, *263*, 369−382.
(17) Killian, B. J.; Kravitz, J. Y.; Somani, S.; Dasgupta, P.; Pang, Y.-P.; Gilson, M. K. Configurational Entropy in Protein-Peptide Binding: Computational Study of Tsg101 Ubiquitin E2 Variant Domain with an HIV-Derived PTAP Nonapeptide. *J. Mol. Biol.* **2009**, *389*, 315−335.
(18) Li, D.-W.; Showalter, S. A.; Brüschweiler, R. Entropy Localization in Proteins. *J. Phys. Chem. B* **2010**, *114*, 16036−16044.
(19) Zhou, H.-X.; Gilson, M. K. Theory of Free Energy and Entropy in Noncovalent Binding. *Chem. Rev.* **2009**, *109*, 4092−4107.
(20) Curtis, J. E.; Tarek, M.; Tobias, D. J. Methyl Group Dynamics as a Probe of the Protein Dynamical Transition. *J. Am. Chem. Soc.* **2004**, *126*, 15928−15929.
(21) Best, R. B.; Clarke, J.; Karplus, M. The Origin of Protein Sidechain Order Parameter Distributions. *J. Am. Chem. Soc.* **2004**, *126*, 7734−7735.
(22) Hu, H.; Hermans, J.; Lee, A. L. Relating Side-Chain Mobility in Proteins to Rotameric Transitions: Insights from Molecular Dynamics Simulations and NMR. *J. Biomol. NMR* **2005**, *32*, 151−162.
(23) Collins, J. R.; Burt, S. K.; Erickson, J. W. Flap Opening in HIV-1 Protease Simulated by Activated Molecular Dynamics. *Nat. Struct. Mol. Biol.* **1995**, *2*, 334−338.
(24) Ishima, R.; Freedberg, D. I.; Wang, Y.-X.; Louis, J. M.; Torchia, D. A. Flap Opening and Dimer-Interface Flexibility in the Free and Inhibitor-Bound HIV Protease, and their Implications for Function. *Structure* **1999**, *7*, 1047−1055.
(25) Hornak, V.; Okur, A.; Rizzo, R. C.; Simmerling, C. HIV-1 Protease Flaps Spontaneously Open and Reclose in Molecular Dynamics Simulations. *Proc. Natl. Acad. Sci. U.S.A.* **2006**, *103*, 915−920.
(26) Trylska, J.; Tozzini, V.; Chang, C.-e. A.; McCammon, J. A. HIV-1 Protease Substrate Binding and Product Release Pathways Explored with Coarse-Grained Molecular Dynamics. *Biophys. J.* **2007**, *92*, 4179−4187.
(27) Phillips, J. C.; Braun, R.; Wang, W.; Gumbart, J.; Tajkhorshid, E.; Villa, E.; Chipot, C.; Skeel, R. D.; Kale, L.; Schulten, K. Scalable Molecular Dynamics with NAMD. *J. Comput. Chem.* **2005**, *26*, 1781−1802.
(28) MacKerell, A. D.; Bashford, D.; Bellott, M.; Dunbrack, R. L.; Evanseck, J. D.; Field, M. J.; Fischer, S.; Gao, J.; Guo, H.; Ha, S.; et al. All-Atom Empirical Potential for Molecular Modeling and Dynamics Studies of Proteins. *J. Phys. Chem. B* **1998**, *102*, 3586−3616.
(29) Jorgensen, W. L.; Chandrasekhar, J.; Impey, J. D. M.; Rw; Klein, M. L. Comparison of Simple Potential Functions for Simulating Liquid Water. *J. Chem. Phys.* **1983**, *79*, 926−935.
(30) Heaslet, H.; Rosenfeld, R.; Giffin, M.; Lin, Y.-C.; Tam, K.; Torbett, B. E.; Elder, J. H.; McRee, D. E.; Stout, C. D. Conformational Flexibility in the Flap Domains of Ligand-Free HIV Protease. *Acta Crystallogr.* **2007**, *D63*, 866−875.
(31) Rayner, M. M.; Cordova, B. C.; Meade, R. P.; Aldrich, P. E.; Jadhav, P. K.; Ru, Y.; Lam, P. Y. DMP 323, a Nonpeptide Cyclic Urea Inhibitor of Human Immunodeficiency Virus (HIV) Protease, Specifically and Persistently Blocks Intracellular Processing of HIV Gag Polyprotein. *Antimicrob. Agents Chemother.* **1994**, *38*, 1635−1640.
(32) Lam, P. Y. S.; Ru, Y.; Jadhav, P. K.; Aldrich, P. E.; DeLucca, G. V.; Eyermann, C. J.; Chang, C.-H.; Emmett, G.; Holler, E. R.; Daneker, W. F.; et al. Cyclic HIV Protease Inhibitors: Synthesis, Conformational Analysis, P2/P2′ Structure Activity Relationship, and Molecular Recognition of Cyclic Ureas. *J. Med. Chem.* **1996**, *39*, 3514−3525.
(33) Chemical Computing Group Inc., *MOE (Molecular Operating Environment)*, 2009.
(34) Yamazaki, T.; Nicholson, L. K.; Torchia, D. A.; Wingfield, P.; Stahl, S. J.; Kaufman, J. D.; Eyermann, C. J.; Hodge, C. N.; Lam, P. Y. S.; Ru, Y.; et al. NMR and X-Ray Evidence that the HIV Protease Catalytic Aspartyl Groups are Protonated in the Complex Formed by the Protease and a Non-Peptide Cyclic Urea-Based Inhibitor. *J. Am. Chem. Soc.* **1994**, *116*, 10791−10792.
(35) MacKerell, A. D. CHARMM FF Parameters. http://mackerell.umaryland.edu/CHARMM_ff_params.html (accessed in 2009).
(36) Frisch, M. J.; Trucks, G. W.; Schlegel, H. B.; Scuseria, G. E.; Robb, M. A.; Cheeseman, J. R.; Montgomery, J. A., Jr.; Vreven, T.; et al. *Gaussian 03*; Gaussian, Inc.: Wallingford, CT, 2004.
(37) Prompers, J. J.; Bruschweiler, R. General Framework for Studying the Dynamics of Folded and Nonfolded Proteins by NMR Relaxation Spectroscopy and MD Simulation. *J. Am. Chem. Soc.* **2002**, *124*, 4522−4534.
(38) Prompers, J. J.; Bruschweiler, R. Reorientational Eigenmode Dynamics: A Combined MD/NMR Relaxation Analysis Method for Flexible Parts in Globular Proteins. *J. Am. Chem. Soc.* **2001**, *123*, 7305−7313.
(39) Nicholson, L. K.; Yamazaki, T.; Torchia, D. A.; Grzesiek, S.; Bax, A.; Stahl, S. J.; Kaufman, J. D.; Wingfield, P. T.; Lam, P. Y. S.; Jadhav,

P. K.; et al. Flexibility and Function in HIV-1 Protease. *Nat. Struct. Biol.* **1995**, *2*, 274−280.
(40) Tjandra, N.; Wingfield, P.; Stahl, S.; Bax, A. Anisotropic Rotational Diffusion of Perdeuterated HIV Protease from N-15 NMR Relaxation Measurements at Two Magnetic Fields. *J. Biomol. NMR* **1996**, *8*, 273−284.
(41) Freedberg, D. I.; Ishima, R.; Jacob, J.; Wang, Y. X.; Kustanovich, I.; Louis, J. M.; Torchia, D. A. Rapid Structural Fluctuations of the Free HIV Protease Flaps in Solution: Relationship to Crystal Structures and Comparison with Predictions of Dynamics Calculations. *Protein Sci.* **2002**, *11*, 221−232.
(42) Ishima, R.; Louis, J. M.; Torchia, D. A. Characterization of Two Hydrophobic Methyl Clusters in HIV-1 Protease by NMR Spin Relaxation in Solution. *J. Mol. Biol.* **2001**, *305*, 515−521.
(43) Krishnan, M.; Smith, J. C. Reconstruction of Protein Side-Chain Conformational Free Energy Surfaces From NMR-Derived Methyl Axis Order Parameters. *J. Phys. Chem. B* **2012**, *116*, 4124−4133.
(44) Chatfield, D. C.; Szabo, A.; Brooks, B. R. Molecular Dynamics of Staphylococcal Nuclease: Comparison of Simulation with 15N and 13C NMR Relaxation Data. *J. Am. Chem. Soc.* **1998**, *120*, 5301−5311.
(45) Lee, A. L.; Wand, A. J. Microscopic Origins of Entropy, Heat Capacity and the Glass Transition in Proteins. *Nature* **2001**, *411*, 501−504.